Structure and Infrastructure Engineering. 10(3), 328-345 (2014)

Feasibility investigation for a bridge damage identification method through moving vehicle laboratory experiment

K.C. Chang [a] , C.W. Kim [b,*] , and M. Kawatani [c]

[a,b] *Dept. of Civil and Earth Resources Engineering, Kyoto University, Kyoto, Japan;*
[c] *Dept. of Civil Engineering, Kobe University, Kobe, Japan*

(Received ???; final version received ???)

Abstract

This paper investigated the feasibility of the pseudo-static damage identification method derived from a bridge-vehicle interaction system through a moving vehicle laboratory experiment. The element stiffness index, defined as the ratio of flexural rigidity of a damaged member to that of an intact member, serves as the damage indicator. Three vehicle models and two travelling speeds were considered in the experiment to examine the effect of vehicle's dynamic characteristic and traveling speed on identified results. It is demonstrated that locations and severities of damages are detectable using the proposed method in spite of the probable changes of roadway roughness and environmental conditions. In addition, adopting higher vehicle speed as well as the vehicle with frequency close to that of the bridge increased the probability of detecting damages.

Keywords: bridge health monitoring (BHM); bridge-vehicle interaction; pseudo-static damage identification; element stiffness index; moving vehicle; laboratory experiment

* Corresponding author. Email: kim.chulwoo.5u@kyoto-u.ac.jp

1. Introduction

The potential economic and life-safety implications of early diagnosis investigation in structures have motivated a considerable number of researches into structural health monitoring (e.g., Rizos *et al*. 1990, Shifrin and Ruotolo 1999, Adeli and Jiang 2006, Siringoringo and Fujino 2006, Ni *et al*. 2008). It is also intended to provide very rapidly and reliable information related to structural health condition.

Structures in many engineering fields are examined through periodic monitoring with the intention of minimizing the safety risk on the one hand and lowering maintenance costs to the greatest extent on the other hand by carrying out maintenance activities at appropriate times (Estes and Frangopol 1999, Wenzel and Pichler 2005, Yang et al. 2005). Moreover structural health monitoring is useful for rapid condition screening after a seismic event especially for countries with frequent earthquakes.

Many precedent studies particularly addressing vibration-based damage detection methods have specifically examined global change of modal properties and parameters of bridge structures. The fundamental concept behind this technology is that a change in physical properties, such as reduced stiffness resulting from damage, will change these modal properties detectably (Rizos *et al*. 1990, Salawu 1997, Shifrin and Ruotolo 1999, Fan and Qiao 2011). Ambient excitations, such as wind and traffic loadings, are adopted in many related studies.

For bridges with a long span, wind-induced vibrations are important dynamic sources (e.g., Ni *et al*. 2008). Even seismic records have been used for system identification of a cable-stayed bridge (Siringoringo and Fujino 2006). In addition, an important problem that must be solved in health monitoring of short span bridges which

are insensitive (or sometimes impassive) to the wind load is how to excite the bridge economically, reliably, and rapidly. From the periodic monitoring point of view, the earthquake is an unattractive excitation for bridges because of its rare occurrence even in earthquake prone regions. Normal traffic excitations may be important dynamic sources. However, traffic-induced vibration is a kind of nonstationary process that strengthens with decreasing span length.

The following study is an attempt to use traffic-induced vibrations for damage identification of bridges. In particular the study is based on an algorithm derived from a bridge-vehicle interaction system which has been developed in order to investigate nonstationarity of the traffic-induced vibration of bridges.

Actually many researches are focusing on the bridge-vehicle interaction problem in order to clarify the influence of excitations from moving vehicles on bridge damage. Common analytical approaches for the bridge-vehicle interaction problem are based on one-dimensional or two-dimensional models of bridges and vehicles (e.g., Hutton and Cheung 1979, Hino *et al*. 1985, Inbahathan and Wieland 1987, Fryba 1996, Green and Cebon 1997, Lou and Zeng 2005). Nevertheless there are a few three-dimensional analytical models (e.g., Mulcahy 1983, Kou and DeWolf 1997, Huang and Wang 1998, Kim *et al*. 2005).

However, only a few studies have been focused on the bridge-vehicle interaction for BHM so far. An attempt for the identification of bridge frequencies indirectly from the dynamic responses of a moving vehicle was reported by Yang *et al*. (2004). In the study, a moving vehicle is treated as a message carrier of dynamic properties of bridges through the bridge-vehicle interaction. Although to extract the fundamental bridge frequency from the moving vehicle is verified to be feasible, to identify damage location and severity of the bridge with this approach is not of their concern.

The first part of this paper is the introduction of the method for detecting damages from an already developed pseudo-static formulation for the bridge-vehicle interaction system in order to detect damages by a vehicle with a tandem axle (Kim and Kawatani 2008). The major goal of the consecutive study is the verification of the feasibility by a moving vehicle laboratory experiment. To achieve this goal, the methodology presented by Kim and Kawatani (2008) is adopted in this study, except that the vehicle model is slightly revised to match the experiment vehicle. More specifically speaking, the previous study considers the dump truck with tandem axle, whereas the experimental vehicle in this study does not equip the tandem axle. It follows that the derivations are slightly revised, with more details given herein. The Tikhonov regularization method (Tikhonov and Arsenin 1977) is adopted to solve the linear system of equations derived from the pseudo-static formulation, and also to cope with any possible ill-posed problems.

Second, this paper describes details of a moving vehicle laboratory experiment, which is conducted to verify the validity of the method. Then, damage identification results using the experimental data are discussed. Finally it summarizes observations through the experimental study and makes some concluding remarks including future works.

2. Equations of motion for vehicle and bridge

2.1 Equations of motion for a moving vehicle on a bridge

In the moving vehicle laboratory experiment which is described later, the two-axle vehicle model with two degrees of freedom (2DOFs) is used as the experiment vehicle. A schematic figure for bridge-vehicle interaction including a 2DOF sprung mass model

and roadway surface roughness is shown in Figure 1, where $z_v(t)$ and $\theta_{vy}(t)$ respectively denote vehicle's bounce and pitching motions, m_v the vehicle mass, k_{vs} and c_{vs} respectively the spring constant and damping coefficient at the s-th axle of the vehicle. The subscript s indicates the position of an axle: with s = 1 and s = 2 respectively signify the first (or front) and second (or rear) axles. Distances from the vehicle's center of gravity to respective axles are denoted by λ_{x1} and λ_{x2}. $z_0(x_s(t))$ indicates the roadway surface roughness at a position of $x_s(t)$ from the reference position which is assumed as the abutment.

[Figure 1 near here]

Equations of motion for the 2DOF sprung mass model can be formulated as

$$m_v \ddot{z}_v(t) + \sum_{s=1}^{2} \left\{ c_{vs}\dot{\delta}_s(t) + k_{vs}\delta_s(t) \right\} = 0 \tag{1}$$

$$m_v \lambda_{x1}\lambda_{x2}\ddot{\theta}_{vy}(t) - \sum_{s=1}^{2} (-1)^s \lambda_{xs} \left\{ c_{vs}\dot{\delta}_s(t) + k_{vs}\delta_s(t) \right\} = 0 \tag{2}$$

Therein the variable $\delta_s(t)$ denotes the relative vertical displacement at the s-th axle of the vehicle and is defined as

$$\delta_s(t) = z_v(t) - (-1)^s \lambda_{xs}\theta_{vy}(t) - \left\{ w(x_s(t), t) - z_0(x_s(t)) \right\} \tag{3}$$

where the variable $w(x_s(t), t)$ represents the time-variant displacement of the bridge at the contact point of the tire location $x_s(t)$ with respect to the reference position.

2.2 Equations of motion for a bridge under a moving vehicle

A bridge can be conceptually discretized into segments of constant mass density,

stiffness, and length, where each segment can be idealized as a beam, as shown in Figure 1. The characteristics, [ ], [ ], [ ], and [ ], indicated in Figure 1, respectively denote vertical displacements and rotation angles at the left-end and right-end of the *e*-th segment, and the characteristics [ ], [ ], [ ], and [ ] respectively denote the vertical displacement and rotation angle at the (*j*-1)-th and *j*-th nodes of the bridge structure.

Equations of motion for a bridge in a matrix formation are as follows

$$\mathbf{M}_b\ddot{\mathbf{q}}_b(t) + \mathbf{C}_b\dot{\mathbf{q}}_b(t) + \mathbf{K}_b\mathbf{q}_b(t) = \mathbf{f}_b(t), \tag{4}$$

where $\mathbf{M}_b \in \mathbb{R}^{n\times n}$, $\mathbf{C}_b \in \mathbb{R}^{n\times n}$ and $\mathbf{K}_b \in \mathbb{R}^{n\times n}$ respectively represent the mass, damping, and stiffness matrices of the bridge, $\mathbf{q}_b(t) \in \mathbb{R}^n$ the displacement vector, $\mathbf{f}_b(t) \in \mathbb{R}^n$ the force vector of the bridge attributable to a moving vehicle, in which n is the number of degrees of freedom of the bridge, and overdots denote derivatives with respect to time. Herein, Rayleigh damping is adopted to formulate the damping matrices, i.e. the linear combination of mass and stiffness matrices.

It must be noted that the measurement of all DOFs is not feasible from an experimental perspective. In particular the limiting issue for a common use of equations of motion in BHM is the accessibility of rotational angles. The System Equivalent Reduction Expansion Process (SEREP) as a matrix reduction technique (O'Callahan *et al*. 1989) is used to overcome this difficulty. Generally, vehicular loadings are imparted vertically on the bridge. Therefore, the DOF relating to the vertical direction is taken as the retained one. With SEREP, the equations of motion for the bridge are classifiable into sub-matrices and vectors relating to the retained and truncated degrees of freedom as follows

$$\begin{bmatrix} \mathbf{M}_{rr} & \mathbf{M}_{rt} \\ \mathbf{M}_{tr} & \mathbf{M}_{tt} \end{bmatrix} \begin{Bmatrix} \ddot{\mathbf{q}}_r(t) \\ \ddot{\mathbf{q}}_t(t) \end{Bmatrix} + \begin{bmatrix} \mathbf{C}_{rr} & \mathbf{C}_{rt} \\ \mathbf{C}_{tr} & \mathbf{C}_{tt} \end{bmatrix} \begin{Bmatrix} \dot{\mathbf{q}}_r(t) \\ \dot{\mathbf{q}}_t(t) \end{Bmatrix} + \begin{bmatrix} \mathbf{K}_{rr} & \mathbf{K}_{rt} \\ \mathbf{K}_{tr} & \mathbf{K}_{tt} \end{bmatrix} \begin{Bmatrix} \mathbf{q}_r(t) \\ \mathbf{q}_t(t) \end{Bmatrix} = \begin{Bmatrix} \mathbf{f}_r(t) \\ \mathbf{0} \end{Bmatrix}, \tag{5}$$

where subscripts *r* and *t* respectively denote the retained and truncated DOFs; that is, $\mathbf{q}_r(t) \in \mathbb{R}^{nr}$ is the retained DOFs, and remaining truncated DOFs are denoted as $\mathbf{q}_t(t) \in \mathbb{R}^{nt}$, in which superscripts *nr* and *nt* respectively represent the numbers of retained DOFs and truncated ones. In addition, $\mathbf{f}_r(t) \in \mathbb{R}^{nr}$ is the force vector relating to wheel loads of the vehicle; $\mathbf{0} \in \mathbb{R}^{nt}$ is the null vector.

Eigenvectors are also partitioned into the retained and truncated DOFs as (O'Callahan *et al*. 1989)

$$\mathbf{\Phi} = \begin{bmatrix} \mathbf{\Phi}_{rr} & \mathbf{\Phi}_{rt} \\ \mathbf{\Phi}_{tr} & \mathbf{\Phi}_{tt} \end{bmatrix}, \tag{6}$$

where $\mathbf{\Phi}_{rr}$ is the mode to be retained and $\mathbf{\Phi}_{tt}$ is the mode to be truncated.

If matrix $\mathbf{U} \in \mathbb{R}^{n \times nr}$ gives the transformation operator connecting the position of the system DOFs with the retained ones, and $\mathbf{I} \in \mathbb{R}^{nr \times nr}$ denotes the identity matrix, then the transformation operator **U** can be written as

$$\mathbf{U} = \begin{Bmatrix} \mathbf{I} \\ \mathbf{\Phi}_{tr}\mathbf{\Phi}_{rr}^{-1} \end{Bmatrix}. \tag{7}$$

Equation (4) is transformed to the retained coordinates as

$$\mathbf{M}_{br}\ddot{\mathbf{q}}_r(t) + \mathbf{C}_{br}\dot{\mathbf{q}}_r(t) + \mathbf{K}_{br}\mathbf{q}_r(t) = \mathbf{f}_{br}(t). \tag{8}$$

The corresponding system matrices $\mathbf{M}_{br} \in \mathbb{R}^{nr \times nr}$, $\mathbf{C}_{br} \in \mathbb{R}^{nr \times nr}$, $\mathbf{K}_{br} \in \mathbb{R}^{nr \times nr}$ and the force vector $\mathbf{f}_{br} \in \mathbb{R}^{nr}$ are given as

$$\mathbf{M}_{br} = \mathbf{U}^T\mathbf{M}_b\mathbf{U};\ \mathbf{C}_{br} = \mathbf{U}^T\mathbf{C}_b\mathbf{U};\ \mathbf{K}_{br} = \mathbf{U}^T\mathbf{K}_b\mathbf{U};\ \text{and}\ \mathbf{f}_{br}(t) = \mathbf{U}^T\mathbf{f}_b(t). \tag{9}$$

In comparing Equation (8) with Equation (4), $\mathbf{q}_b(t)$ and $\mathbf{q}_r(t)$ have the following relation.

$$\mathbf{q}_b(t) = \mathbf{U}\mathbf{q}_r(t) \tag{10}$$

The force vector $\mathbf{f}_b(t)$ is obtainable from wheel loads as

$$\mathbf{f}_b(t) = \sum_{s=1}^{2} \boldsymbol{\psi}_s(t) P_s(t) \quad , \tag{11}$$

Therein, $\boldsymbol{\psi}_s(t)$ is a load distribution vector to each node of the element on which a tire contacts, and is defined as

$$\boldsymbol{\psi}_s(t) = \left\{ 0;\cdots;0;\psi_s^L(t);\psi_s^R(t);0;\cdots;0 \right\} \in \mathbb{R}^N, \tag{12}$$

where $\psi_s^L(t) = \{x_e^R - x_s(t)\}/l_e$; $\psi_s^R = \{x_s(t) - x_e^L\}/l_e$; l_e is the length of the *e*-th element; and x_e^L and x_e^R respectively indicate the longitudinal coordinates of left end and right end of the *e*-th element (see also Figure 1). $P_s(t)$ denotes the wheel load at a tire and is definable as

$$P_s(t) = \left(1 - \frac{\lambda_{xs}}{\lambda_x}\right) m_v g + c_{vs}\dot{\delta}_s(t) + k_{vs}\delta_s(t) \,. \tag{13}$$

where, $\delta_s(t)$ is the relative vertical displacement at an axle, as shown in Equation (3).

A noteworthy point relating to the equation for $\delta_s(t)$ is that finite element method does not always provide the displacement $w(x_s(t), t)$ at a certain position of a tire because, in general, responses of a bridge model are estimated using the finite element method at each node. Therefore, a linear displacement shape function which is obtainable from a transpose of the load distribution vector shown in Equation (12) is adopted to interpolate the displacement at a certain position $w(x_s(t), t)$ as

$$w(x_s(t), t) = \boldsymbol{\psi}_s^T \mathbf{q}_b(t) \,, \tag{14}$$

where $\boldsymbol{\psi}_s^T(t)$ indicates the vector for the linear displacement shape function of the bridge.

By substituting Equation (10) into Equation (14), the relative displacement at an axle *s* of the vehicle in Equation (3) is rewritable as

$$\delta_s(t) = z_v(t) - (-1)^s \lambda_{xs} \theta_{vy}(t) - \left\{ \boldsymbol{\psi}_s^T \mathbf{U} \mathbf{q}_r(t) - z_0(x_s(t)) \right\}. \tag{15}$$

The combination of the interaction force at a contact point provides equations of motion for a bridge-vehicle interaction system. Using equations from Equation (8) to Equation (15), equations of motion for a bridge under a moving vehicle can be reproduced as

$$\begin{aligned}
&\mathbf{M}_{br} \ddot{\mathbf{q}}_r(t) + \left\{ \mathbf{C}_{br} + \mathbf{U}^T \sum_{s=1}^{2} \boldsymbol{\psi}_s(t) c_{vs} \boldsymbol{\psi}_s^T(t) \mathbf{U} \right\} \dot{\mathbf{q}}_r(t) + \left\{ \mathbf{K}_{br} + \mathbf{U}^T \sum_{s=1}^{2} \boldsymbol{\psi}_s(t) k_{vs} \boldsymbol{\psi}_s^T(t) \mathbf{U} \right\} \mathbf{q}_r(t) \\
&- \mathbf{U}^T \sum_{s=1}^{2} \boldsymbol{\psi}_s(t) c_{vs} \left\{ \dot{z}_v(t) - (-1)^s \lambda_{xs} \dot{\theta}_{vy}(t) \right\} - \mathbf{U}^T \sum_{s=1}^{2} \boldsymbol{\psi}_s(t) k_{vs} \left\{ z_v(t) - (-1)^s \lambda_{xs} \theta_{vy}(t) \right\} \\
&= \mathbf{U}^T \sum_{s=1}^{2} \boldsymbol{\psi}_s(t) \left[\left(1 - \frac{\lambda_{xs}}{\lambda_x} \right) m_v g + \left\{ c_{vs} \dot{z}_0(x_s(t)) + k_{vs} z_0(x_s(t)) \right\} \right]
\end{aligned} \tag{16}$$

A noteworthy point in Equation (16) is that the system damping and stiffness matrices consist of time-variant coefficients, indicating that the traffic-induced vibration of bridges is a nonstationary problem. Therefore, in analyzing such a problem, adopting the damage identification methods subjected to a stationary assumption may mislead to unexpected results. In contrast, the following pseudo-static damage identification method, a time domain analysis method that removes the stationary assumption, may serve as a more proper tool.

3. Pseudo-static damage identification

The concept for the BHM described in this paper is based on the fact that the mechanical properties of the bridge structure may decay due to possible degradation processes and it is often represented by a decrease of stiffness (Dilena and Morassi 2011). This change is detectable by measuring dynamic responses under an inspection vehicle whose dynamic wheel loads or dynamic properties are known. In general, for

simplification the mass matrix of a bridge can be assumed to be unaffected by damage. The damping matrix is affected by the change of stiffness because of the used Rayleigh damping. In addition, the initial parameters of the intact bridge and vehicle model are estimated in a first approach.

The subtraction of linear stiffness equations from Equation (16) yields to the pseudo-static formulation Equation (17), which shows the change of a bridge structure's stiffness as follows:

$$\mathbf{K}_{br}\mathbf{q}_r(t) = \mathbf{f}(t),\ \mathbf{f}(t) \in \mathbb{R}^{nr} \tag{17}$$

where the force vector is defined as

$$\mathbf{f}(t) = \mathbf{f}_{br}(t) + \mathbf{f}_{bb}(t), \tag{18}$$

and pertain follow as

$$\mathbf{f}_{br}(t) = \mathbf{U}^T \sum_{s=1}^{2} \boldsymbol{\psi}_s(t) P_s(t) = \mathbf{U}^T \sum_{s=1}^{2} \boldsymbol{\psi}_s(t) \left\{ \left(1 - \frac{\lambda_{xs}}{\lambda_x} \right) m_v g + c_{vs}\dot{\delta}_s(t) + k_{vs}\delta_s(t) \right\} \tag{19}$$

$$\mathbf{f}_{bb}(t) = -\left(\mathbf{M}_{br}\ddot{\mathbf{q}}_r(t) + \mathbf{C}_{br}\dot{\mathbf{q}}_r(t) \right) \tag{20}$$

The force vector $\mathbf{f}_{br}(t)$ in Equation (19) is the external force of the vehicle moving on the bridge (see also Equation (9)). The measured wheel load is used directly for $\mathbf{f}_{br}(t)$ if measured wheel loads are available by any feasible mean, e.g. see OECD(1998). In other way, without directly measuring wheel loads, the force vector $\mathbf{f}_{br}(t)$ can be calculated using measured acceleration responses of the front and rear axles as follows:

$$\mathbf{f}_{br}(t) = \mathbf{U}^T \sum_{s=1}^{2} \boldsymbol{\psi}_s(t) \left\{ \left(1 - \frac{\lambda_{xs}}{\lambda_x} \right) \left(g - \ddot{z}_{vs}(t) \right) \right\} m_v \tag{21}$$

Details of the derivation are given in Appendix. Therein, $\ddot{z}_{vs}(t)$ which has the relation of $\ddot{z}_{vs}(t) = \ddot{z}_v(t) - (-1)^s(\lambda_x - \lambda_{xs})\ddot{\theta}_{vy}(t)$ indicates the acceleration response at the *s*-th axle of the vehicle.

The change of stiffness $\mathbf{K}_{br}$ in Equation (17) provides information about the change of the bridge's health condition. Detection of the change in $\mathbf{K}_{br}$ is the basic concept of the damage identification methodology proposed in this paper.

The reduced structural stiffness matrix $\mathbf{K}_{br}$ is obtainable using the assembly operator $\mathbf{L}_e$ as

$$\mathbf{K}_{br} = \mathbf{U}^T \left(\sum_{e=1}^{M} \mathbf{L}_e^T \mathbf{K}_{be}^g \mathbf{L}_e \right) \mathbf{U} \,. \tag{22}$$

Therein, M is the number of elements; $\mathbf{L}_e \in \mathbb{R}^{2nf \times n}$ provides the assembly operator of an element that transforms the element stiffness matrix to a structural stiffness matrix in which nf denotes the number of DOFs at an element node. $\mathbf{K}_{be}^g \in \mathbb{R}^{2nf \times 2nf}$ is an element stiffness matrix in the global coordinate given by Equation (23).

$$\mathbf{K}_{be}^g = \mathbf{R}_e^T \mathbf{K}_{be}^i \mathbf{R}_e \tag{23}$$

In that equation, $\mathbf{K}_{be}^i \in \mathbb{R}^{2nf \times 2nf}$ is the element stiffness matrix of the intact state. In addition, $\mathbf{R}_e \in \mathbb{R}^{2nf \times 2nf}$ denotes the coordinate transformation matrix.

Assuming that the damage only changes the bending rigidity to simplify the derivation, the damaged element stiffness matrix $\mathbf{K}_{be}^d \in \mathbb{R}^{2nf \times 2nf}$ in local coordinates is given as the following.

$$\mathbf{K}_{be}^d = \left(E_e I_e\right)^d \times \begin{bmatrix} 12/l_e^3 & & sym. & \\ 6/l_e^2 & 4/l_e & & \\ -12/l_e^3 & -6/l_e^2 & 12/l_e & \\ 6/l_e^2 & 2/l_e & -6/l_e^2 & 4/l_e \end{bmatrix} \begin{matrix} w_e^L(t) \\ \theta_e^L(t) \\ w_e^R(t) \\ \theta_e^R(t) \end{matrix} \tag{24}$$

In that expression, $(E_e I_e)^d$ detnotes the bending rigidity of the e-th element.

The change of the element stiffness is obtainable using the element stiffness index (ESI), which is defined as

$$\mu_e = \frac{\mathbf{K}_{be}^{d}}{\mathbf{K}_{be}^{i}} = \frac{(E_e I_e)^{d}}{(E_e I_e)^{i}}, \tag{25}$$

and then

$$\mathbf{K}_{be}^{d} = \mu_e \cdot \mathbf{K}_{be}^{i}, \tag{26}$$

where μ_e is the element stiffness index, and $(E_eI_e)^i$ denotes the bending rigidity of the e-th element of an intact state.

Introducing the relation in Equation (26) into $\mathbf{K}_{be}^{g}$ of Equation (23), then Equation (22) of the structural stiffness matrix for a bridge can be rewritten for a damaged bridge as

$$\mathbf{K}_{br} = \mathbf{U}^T \left(\sum_{e=1}^{M} \mu_e \mathbf{L}_e^T \mathbf{K}_{be}^{g} \mathbf{L}_e \right) \mathbf{U}. \tag{27}$$

A noteworthy point is that the ESI value is unity for an intact bridge, meaning that the value of unity for μ_e (e = 1, …, M) is the reference value for this study.

Substituting the relation in Equation (27) into Equation (17) of the pseudo-static formulation yields

$$\mathbf{U}^T \left(\sum_{e=1}^{M} \mu_e \mathbf{L}_e^T \mathbf{K}_{be}^{g} \mathbf{L}_e \right) \mathbf{U}\mathbf{q}_r(t) = \mathbf{f}(t). \tag{28}$$

Equation (28) is rewritten simply for the governing equation of μ_e as

$$\sum_{e=1}^{M} \mu_e \mathbf{h}_e(t) = \mathbf{f}(t), \tag{29}$$

where $\mathbf{h}_e(t) \in \mathbb{R}^{nr}$ is a coefficient vector of the e-th element at time t. It is defined as

$$\mathbf{h}_e(t) = \left(\mathbf{U}^T \mathbf{L}_e^T \mathbf{K}_{be}^{g} \mathbf{L}_e \mathbf{U} \right) \mathbf{q}_r(t). \tag{30}$$

Equation (29) can be condensed as a matrix formation as follows:

$$\mathbf{H}(t)\mathbf{x} = \mathbf{f}(t) \tag{31}$$

where $\mathbf{x} \in \mathbb{R}^M$ is defined as the vector of ESI of a bridge:

$$\mathbf{x} = \{\mu_1; \quad \mu_2; \quad \cdots \quad \mu_{M-1}; \quad \mu_M\} \tag{32}$$

and $\mathbf{H}(t) \in \mathbb{R}^{nr \times M}$ is defined as the coefficient matrix of a bridge model at time t :

$$\mathbf{H}(t) = \{\mathbf{h}_1(t) \quad \mathbf{h}_2(t) \quad \cdots \quad \mathbf{h}_{M-1}(t) \quad \mathbf{h}_M(t)\} \tag{33}$$

The moving vehicle experiment and measured data of *mt* samples are available in damage identification, then Equation (31) can be written simply as

$$\mathbf{A}\mathbf{x} = \mathbf{b}, \tag{34}$$

where $\mathbf{A} \in \mathbb{R}^{nq \times M}$ is the linear prediction data matrix as offered in Equation (35) with $nq = nr \times mt$.

$$\mathbf{A} = \begin{bmatrix} \mathbf{h}_1(t_0) & \mathbf{h}_2(t_0) & \cdots & \mathbf{h}_M(t_0) \\ \vdots & \vdots & \ddots & \vdots \\ \mathbf{h}_1(t_{mt-1}) & \mathbf{h}_2(t_{mt-1}) & \cdots & \mathbf{h}_M(t_{mt-1}) \end{bmatrix} = \begin{bmatrix} \mathbf{H}(t_0) \\ \vdots \\ \mathbf{H}(t_{mt-1}) \end{bmatrix} \tag{35}$$

In addition, the observation vector $\mathbf{b} \in \mathbb{R}^{nq}$ in Equation (34) is structured as follows:

$$\mathbf{b} = \{\mathbf{f}(t_0); \quad \cdots; \quad \mathbf{f}(t_{mt-1})\}. \tag{36}$$

Equation (34) represents a linear system of equations that can be subtracted from the bridge-vehicle interaction equations of motion and used for damage identification of bridges. The Tikhonov regularization (Tikhonov and Arsenin 1977) is used to solve the equation of linear system shown in Equation (34) as

$$\min \left\{ \left\| \mathbf{A}\mathbf{x} - \mathbf{b} \right\|_2 - \lambda \left\| \mathbf{x} - \mathbf{x}_0 \right\|_2 \right\} \mathbf{A} \in \mathbb{R}^{nq \times M}, \lambda \in [0, \infty]. \tag{37}$$

Therein the first term is the same as that of the ordinary least-squares (OLS) minimization. The second term is the side constraint, which stabilizes the problem and singles out a useful and stable solution. The regularization parameter λ controls the

weight given to minimization of the side constraint relative to minimization of the residual norm. The L-curve method (Hansen 1994) has been used for the problem on hand to choose the optimal regularization parameter. The vector $\mathbf{x}_0$ is the *a priori* estimate. In addition, the unit vector has been selected for the *a priori* estimate because the ESI value of the intact bridge is equal to the unit value.

Finally, the performance of bridge structures is detectable on the results of the ESI vector **x**. Determination of the ESI vector can also provide information related to damage location and severity.

The concept of the above damage identification method has been verified to be feasible through numerical simulations with a slightly sophisticated vehicle model (Kim and Kawatani 2008). In the present study, focus is placed on the feasibility verification through a laboratory experiment, which is introduced as follows.

4. Moving vehicle laboratory experiment

A moving vehicle laboratory experiment was performed to investigate feasibility of the proposed method. The experiment setup is summarized in Figure 2, in which geometry and structural properties of the girder model are shown in Figure 2(a) and Figure 2(b). Regarding damage, two damage scenarios were considered in the experiment: as for the first scenario (hereafter Damage-A), three saw cuts were applied to both left and right sides of web plates between L/4 and L/2 of the bridge model (see Damage Section I in Figure 2(c)); the second damage scenario (hereafter Damage-B) considered both Damage Section I and Damage section II which cuts out a part of the web plate between 3L/4 and L of the bridge as also shown in Figure 2(c). For damaged section I, the bending rigidity of the member decreased to around 89 % of the intact state, and for

damaged section II, it decreased to around 77%. It should be noted that the bridge structure and damage types performed herein are representatives for illustration only, but not confined to specific types. In this feasibility study, the focus is put on verifying the feasibility of the present approach. Therefore, the artificial damages are not intended to perfectly simulate real damages, but to make the bridges serve as damaged samples in comparison to intact ones, in terms of bending rigidity reduction.

[Figure 2 near here] [Table 1 near here]

Natural frequencies and damping constants of the first bending mode of the bridge model are presented in Table 1, where the natural frequencies are taken from free vibration experiments and the damping ratios are estimated from the free vibration time histories after the vehicle leaving the bridge to avoid their dependence on the amplitude. The analytical bridge frequency can be calculated as 2.53 Hz; herein, the natural frequency of the intact bridge was measured as 2.69 Hz, about 6% greater than the analytical one. The slightly larger experimental frequency than the analytical one might be contributed to the following inevitable factors: (1) slight discrepancy between design and manufacture, and (2) the hinge and roller supports not ideally free of rotation. Despite the inevitable factors, the intact scaled bridge still served well as a reference for damage ones. Regarding to the dynamic characteristics, Table 1 shows the decreasing natural frequency of the first bending mode with increasing damage degree. Unlike natural frequency, the damping ratio did not undergo a given pattern.

Roadway profiles were considered in the experiment as actual bridges. Both left and right wheel paths of the vehicle were paved with an electrical tape at the interval of 100mm as shown in Figure 3. Thickness of the tape was 0.2 mm.

[Figure 3 near here] [Figure 4 near here]

The experiment vehicle equipped with data acquisition system is shown in Figure 4. A wireless LAN server was used to transmit vehicle's vibration signals by radio. The experiment vehicle was driven by a guide wire traction system. Although the driven system may introduce some inherent restrictions, e.g. an acceleration section required before the vehicle reaches a design constant speed and the wire vibrations that may slightly affect the vehicle dynamics, the vehicle worked quite well in the experiments, as will be illustrated below. Herein, three different vehicle models were considered, each with different combination of mass and spring to yield different natural frequency of the bounce mode to the others. The properties of the three vehicles, labeled as VT-A, B, and C, are listed in Table 2. The natural frequencies for the three vehicle models were measured as 2.93 Hz, 3.76 Hz and 3.03 Hz. In order to investigate the effect of the vehicle speed on damage identification results, two different speeds of 0.93 and 1.63 m/s were adopted for each vehicle model. Therefore, six loading scenarios were considered, as summarized in Table 3. Previously mentioned vehicle speeds of 0.93 and 1.63 m/s yield to speed parameters α = 0.032 and 0.056, respectively, as follows:

$$\alpha = v/(2\cdot f\cdot l_b) \tag{38}$$

with v = vehicle speed (m/s); f = fundamental frequency of the first bending mode; and l_b = bridge span length (m).

[Table 2 near here] [Table 3 near here]

Several important factors regarding to the scaling of above vehicle and bridge model were considered, including mass ratio and length ratio of the vehicle to the bridge, natural frequencies of the vehicle and bridge, and speed parameter. Let us take VT-A vehicle type for example. The mass ratio of the vehicle to the bridge was designed as 21.6 kg / 291 kg = 7.4%; the length ratio was designed as 400 mm / 5600 mm = 7.1%; the natural frequencies of the vehicle and bridge were measured as 2.93 and 2.69 Hz, as was mentioned above; the speed parameter were designed as 0.031 and 0.054, which is analogous to the speed of 24 km/hr and 42 km/hr, respectively, for a real bridge with a length of 40 m. All those factors were within reasonable ranges, indicating that the scaled vehicle and bridge models were adequate to simulate real vehicle-bridge systems.

The acceleration responses of the bridge were recorded at 1/4, 1/2, and 3/4 of the span length. In addition, two points on front and rear axles of the vehicle served as observation points on the vehicle. The sampling rate of signals was 100Hz.

Time histories of responses at each observation point of the bridge as well as the acceleration response at each axle of the vehicle are shown in Figures 5-7 according to damage scenarios. They are the responses under the loading scenario SCN1, i.e. VT-A type vehicle traveling with speed of 0.93m/s. Fourier amplitude spectra transfered from the acceleration responses of the vehicle during its passage over the bridge are also summarized in those figures.

[Figure 5 near here] [Figure 6 near here] [Figure 7 near here]

It is shown in the case with damage scenario Damage-A that the amplitude of acceleration responses for the bridge was drastically decreased, whereas that for the vehicle was amplified. An interesting point is that the contributions of dominant

frequencies near 2.5Hz and 23.4Hz were weakened by the damage. In the case with damage scenario Damage-B, which included both Damaged Section I and Damage Section II, the acceleration responses of the bridge as well as those of the vehicle had tendency to be amplified with respect to the case with intact bridge. Varied damping constants due to the damage were one reason for the variation of the response amplitude.

5. Experimental Results

5.1 Damage Identification

This chapter is devoted to a discussion of damage identification results from the experimental responses by means of the method proposed in the previous chapter. Discussions in this chapter are divided into three views: possibility of identifying multiple damages on the bridge model; effect of vehicle's dynamic characteristic to identification results; and effect of vehicle's traveling speed to identification results. The identified ESI values for Damage-A and Damage-B, two damage scenarios, are summarized in Figure 8 and Figure 9 respectively. To examine the effect of vehicle type and speed to the identification result, averaged ESI values are summarized according to the vehicle type and traveling speed as shown in Figure 10 and Figure11 respectively. In those figures, the values of actual ESI for the damaged elements, i.e. 0.89 for element No. 2 and 0.77 for element No. 4, are marked in horizontal virtual lines. The difference between the actual and identified ESI's, referred to as the identification error, is also shown.

[Figure 8 near here] [Figure 9 near here]

[Figure 10 near here] [Figure 11 near here]

For Damage-A, the damage on the element No.2 was well identified by the proposed method except SCN3 (see Figure 8), the loading scenario 3, which identified ELEM. No.1 as the most suspected damage member rather than ELEM. No.2. Unfortunately the reason for unsuccessful identification was not clear yet. The percentage terms in the figures denote the error relating to identifying severity of damages. The error varied up to 4.5 %, and it demonstrated the proposed method can also presume the damage severity. Although the ESI's are reduced in ELEM. No.1 and 3 probably due to the bridge that acts as a continuum system, the proposed method is still regarded as an effective tool in identifying the most suspected damage member, say ELEM. No.2 in this case. Considering Damage-B, suspected damage locations were also well identified, as shown in Figure 8. The damage severity of each member was identified within the error of 7.0 % for the damaged section I (ELEM. No.2 in Figure 2) and within the error of 8.3 % for the damaged section II (ELEM. No.4 in Figure 2).

For the effect of vehicle types as shown in Figure 10, the vehicle VT-B which has the highest frequency for the bounce motion among three vehicles resulted in the smallest error for indentifying severity. However, the identified damage location was obscure especially for Damage-A. On the other hand, both VT-A and VT-C vehicles which have smaller frequency for the bounce motion and closer frequency with that of bridge's first bending mode gave clear damage locations, and the identification error rate was less than 5.6%. For Damage-B, reasonable identification for damage severity as well as damage locations was observed without being greatly affected by the vehicle type.

The effect of vehicle's travelling speed to the identification accuracy is shown in Figure 11. For Damage-A, the lower travelling speed, v=0.93m/s, gave smaller error for

identifying damage severity than that under vehicle speed of 1.63m/s. However, the damage location became unclear under the lower speed. For Damage-B, both travelling speeds resulted reasonable identification for damage severity as well as damage locations.

Observations from the experimental investigation demonstrated that locations and severities of damage were generally identified without great variation according to vehicle type and speed, even though the vehicle with similar frequency characteristics with bridge's fundamental frequency and higher speed might give better chance to identify both severity and location. One thing noteworthy is that damages were successfully identified in spite of the probable changes of the artificial roadway profiles and support condition occurring at the work of cutting the girder.

The identified results herein can be compared with those obtained from another modal-based study performed by Kim et al. (2012) on the same bridge and vehicle model. In that study, the modal parameters of both the intact and damaged bridges were identified from the vehicle-induced bridge vibrations by the multivariate AR model. Their results showed that the changes of the first three dominant frequencies and damping ratios can be identified under a moving vehicle with a low speed and serve as valuable indications for bridge health monitoring. However, the damage location and severity were not mentioned. In a higher vehicle speed, the identified bridge frequency is far from the bridge's natural frequency since vehicle-bridge interaction becomes dominant according to the vehicle speed. In compared with the previous modal-based method, the present method shows its effectiveness in the identification of the damage location and severity, as has been discussed above.

5.2 Sensitivity Analysis on Damage Severity

To realize the sensitivity of the present method to the damage severity, an independent sensitivity analysis is performed with the same scaled bridge and vehicle VT-A. Another roadway surface profile of rougher level is applied on the bridge, as shown in Fig. 12. The damage severity is applied by cutting different depths of the girder flange between 3L/8 and L/2 span (in ELEM. No. 2): 5 mm for light damage (designated as D1), 10 mm for medium damage (D2), and 15 mm for severe damage (D3). The cuts on the bridge make the bending rigidity of the damaged section decrease to 94%, 80%, and 65%, respectively, of the intact one. In this sensitivity study, only traffic scenario SCN1 is considered. Other traffic scenarios may show similar trends.

[Figure 12 near here] [Figure 13 near here]

Figure 13 shows the identified ESI for the three damage cases D1 to D3. It is observed that ELEM. No. 2 is identified as the most suspicious element for all cases and the identified ESI decreases as the damage severity increases, verifying the effectiveness of the present method in identifying damage location and relative damage severity. Table 4 summarizes the identified ESI's and absolute errors of ELEM. No. 2. Except for case D3, the other two cases show acceptable absolute errors in identified ESI, implying that the absolute damage severity can be identified by the present method within the error of 6.0% even for a light damage. However, most of the errors of ESI in this sensitivity study are greater than those obtained in Sec. 5.1, probably due to the rougher roadway surface. The potential reason for such slightly unstable ESI results requires further investigations.

6. Conclusions

This paper presents a moving vehicle laboratory experiment of a bridge model to investigate feasibility of bridge damage identification using the pseudo-static approach derived from a vehicle-bridge interaction system, especially focused on short span bridges because of their great contribution to entire infrastructure system. The element stiffness index (ESI), which defines the normalized changes in the element stiffness, is adopted as an indicator of damage.

The experimental study demonstrated that damage location and severity are well detectable using the proposed method except one case, SCN3, of which reason is not clarified yet. Better chance to detect damage was observed by adopting higher vehicle speed as well as by using the vehicle with the frequency closer to that of the experimental bridge. However, locations and severities of damage were generally identified without great variation with respect to vehicle type and speed. Moreover, damages were still successfully identified in spite of the probable changes of the artificial roadway profiles and support condition occurring at the work of cutting the girder. From an independent sensitivity study, the effectiveness of the present method in identifying damage location and relative damage severity is verified, even for a light damage case.

The most important and fundamental result obtained through this study is the potential feasibility of the method for addressing real-world problems. Many further investigations are necessary to make the method practically applicable, such as how sensitive the present approach is under various kinds of damages, and the accuracy with respect to the bending rigidity reduction ratio. Another great challenge is realizing data acquisition both from moving vehicle and bridge simultaneously. Wireless sensing may

be a solution. The school of remaining problems is a strong motivation for the next challenge

Acknowledgements

A part of this study is supported by the Japan Society for the Promotion of Science (Grant-in-Aid for Exploratory Research under project No.19656112 and Grant-in-Aid for Scientific Research (C) under project No. 20560443), and the first author is sponsored partly by the National Science Council, Taiwan (Grant No. NSC 100-2917-I-564-052). Such financial aids are gratefully acknowledged.

Appendix

To show that Equation (21) is equivalent to Equation (19), $V_s(t)$ is newly defined as

$$V_s(t) = c_{vs}\dot{\delta}_s(t) + k_{vs}\delta_s(t)\,. \tag{A1}$$

Using Equation (A4), $P_s(t)$ of Equation (13) is rewritable as

$$P_s(t) = \left(1-\frac{\lambda_{xs}}{\lambda_x}\right)m_v g + c_{vs}\dot{\delta}_s(t) + k_{vs}\delta_s(t) = \left(1-\frac{\lambda_{xs}}{\lambda_x}\right)m_v g + V_s(t)\,. \tag{A2}$$

Substituting Equation (A1) into Eqs. (1) and (2) yields the following relations.

$$m_v\ddot{z}_v(t) + V_1(t) + V_2(t) = 0 \tag{A3}$$

$$m_v\lambda_{x1}\lambda_{x2}\ddot{\theta}_{vy}(t) + \lambda_{x1}V_1(t) - \lambda_{x2}V_2(t) = 0 \tag{A4}$$

Solving simultaneous linear equations of Equation (A3) and Equation (A4) for $V_1(t)$ and $V_2(t)$, the $V_s(t)$ in terms of acceleration responses using the relationship $\lambda_x = \lambda_{x1} + \lambda_{x2}$ is obtainable as

$$V_s(t) = -\frac{\lambda_x - \lambda_{xs}}{\lambda_x}\left(\ddot{z}_v(t) - (-1)^s\lambda_{xs}\ddot{\theta}_{vy}(t)\right)\,m_v\,. \tag{A5}$$

$\ddot{z}_{vs}(t)$ denotes the acceleration response at the s-th axle (s = 1 and 2, respectively, for the first (or front) and second (or rear) axles). Therefore Equation (A5) is rewritable as

$$V_s(t) = -\frac{\lambda_x - \lambda_{xs}}{\lambda_x}\ddot{z}_{vs}(t)m_v = -\left(1-\frac{\lambda_{xs}}{\lambda_x}\right)\ddot{z}_{vs}(t)m_v\,. \tag{A6}$$

Substituting Equation (A6) into Equation (A2), the wheel load using the acceleration measured at each axle is definable as

$$P_s(t) = \left\{\left(1-\frac{\lambda_{xs}}{\lambda_x}\right)\left(g - \ddot{z}_{vs}(t)\right)\right\}m_v\,. \tag{A7}$$

It indicates that Equation (A7) is equivalent to Equation (A2) (or Equation (13)). Therefore, it confirms that Equation (21) is equivalent to Equation (19).

References

Adeli, H. and Jiang, X., 2006. Dynamic fuzzy wavelet neural network model for structural system identification. *Journal of Structural Engineering, ASCE*, 132 (1), 102-111.

Dilena, M. and Morassi, A., 2011. Dynamic testing of a damaged bridge. *Mechanical Systems and Signal Processing*, 25, 1485-1507.

Estes, A.C. and Frangopol, D.M., 1999. Repair optimization of highway bridges using system reliability approach. *Journal of Structural Engineering, ASCE*, 125 (7), 766-775.

Fan, W. and Qiao, P., 2011. Vibration-based damage identification methods: a review and comparative study. *Structural Health Monitoring*, 10, 83-111.

Fryba, L., 1996. *Dynamics of Railway Bridges*, 3rd ed. London: Thomas Telford Ltd.

Green, M.F. and Cebon, D., 1997. Dynamic interaction between heavy vehicles and highway bridges. *Computer and Structures*, 62, 253-264.

Hansen, P.C., 1994. Regularization tools, A Matlab package for analysis and solution of discrete ill-posed problems. *Numerical Algorithms*, 6, 1-35.

Hino, J., Yoshimura, T., and Ananthanarayana, N., 1985. Vibration analysis of non-linear beams subjected to a moving load using the finite element method. *Journal of Sound and Vibration*, 100, 477-491.

Huang, D. and Wang, T.L., 1998. Vibration of highway steel bridges with longitudinal grades. *Computer and Structures*, 69, 235-245.

Hutton, S.G. and Cheung, Y.K., 1979. Dynamic response of single span highway bridges. *Earthquake Engineering and Structural Dynamics*, 7, 543-553.

Inbahathan, M.J. and Wieland, M., 1987. Bridge vibrations due to vehicle moving over rough surface. *Journal of Structural Engineering, ASCE*, 113, 1994-2008.

Kim, C.W., Kawatani, M. and Kim, K.B., 2005. Three-dimensional dynamic analysis for bridge-vehicle interaction with roadway roughness. *Computer and Structures*, 83, 1627-1645.

Kim, C.W. and Kawatani, M., 2008. Pseudo-static approach for damage identification based on coupling vibration with a moving vehicle. *Structure and Infrastructure Engineering*, 4 (5), 371-79.

Kim, C.W., Kawatani, M., and Hao, J., 2012, Modal parameter identification of short span bridges under a moving vehicle by means of multivariate AR model. *Structure and Infrastructure Engineering*, 8 (5), 459-72.

Kou, J.W. and DeWolf, J. T., 1997. Vibrational behavior of continuous span highway bridge – Influencing variables. *Journal of Structural Engineering, ASCE*, 123, 333-344.

Lou, P. and Zeng, Q., 2005. Formulation of equations of motion of finite element form for vehicle-track-bridge interaction system with two types of vehicle model. *International Journal of Numerical Methods in Engineering*, 62, 435-74.

Mulcahy, N.L., 1983. Bridge response with tractor-trailer vehicle loading. *Earthquake Engineering and Structural Dynamics*, 11, 649-665.

Ni, Y.Q., Zhou, H.F., Chan, K.C., and Ko, J. M., 2008. Modal flexibility analysis of cable-stayed bridge Ting Kau bridge for damage identification. *Computer-Aided Civil and Infrastructure Engineering*, 23 (3), 223-236.

O'Callahan, J., Avitabile, P., and Riemer, R., 1989. System equivalent reduction expansion process. *7th International Modal Analysis Conference*, Las Vegas, January, 29-37.

OECD, 1998. *Dynamic Interaction Between Vehicles and Infrastructure Experiment (DIVINE), Technical Report*, DSTI/DOT/RTR/IR6(98)1/FINAL.

Rizos, P.F., Aspragatos, N., and Dimarogonas, A.D., 1990. Identification of crack location and magnitude in a cantilever beam from the vibration modes. *Journal of Sound and Vibration*, 138, 381-388.

Salawu, O.S., 1997. Detection of structural damage through changes in frequency: a review. *Engineering Structures*, 19, 718-723.

Shifrin, E.I. and Ruotolo, R., 1999. Natural frequencies of a beam with an arbitrary number of cracks. *Journal of Sound and Vibration*, 222, 409-423.

Siringoringo, D.M. and Fujino, Y., 2006. Observed dynamic performance of the Yokohama Bay Bridge from system identification using seismic records. *Structural Control and Health Monitoring*, 13, 226-244.

Tikhonov, A.V. and Arsenin, V.Y., 1977. *Solutions of Ill-posed Problems*. New York: Wiley.

Wenzel, H. and Pichler, D., 2005. *Ambient Vibration Monitoring*. New York: John Wiley & Sons.

Yang, S.I., Frangopol, D.M., and Neves, L.C., 2005. Optimum maintenance strategy for deteriorating bridge structures based on lifetime functions. *Engineering Structures*, 28, 196-206.

Yang, Y.B., Lin, C.W., and Yau, J. D., 2004. Extracting bridge frequencies from the dynamic response of a passing vehicle. *Journal of Sound and Vibration*, 272, 471-493.

Table 1. Frequency and damping ratio of the first mode of the bridge model.

Damage scenario	Frequency (Hz)	Damping ratio
Intact	2.69	0.0337
Damage-A	2.59	0.0471
Damage-B	2.54	0.0245

Table 2. Vehicle properties.

Vehicle Type		VT-A	VT-B	VT-C
Mass (kg)	Front axle	5.7	5.7	5.7
	Rear axle	15.9	15.9	20.1
	Sum	21.6	21.6	25.8
Spring constant (N/m)	Front axle	2.00	3.54	3.42
	Rear axle	3.72	6.60	9.54
Damping constant	Front axle	0.057	0.056	0.061
	Rear axle	0.059	0.052	0.064
Natural frequency of bounce motion (Hz)		2.93	3.76	3.03
Axle distance (cm)		40.0	40.0	40.0

Table 3. Loading scenario

Loading scenario	Vehicle type	Vehicle speed (m/s)
SCN1	VT-A	0.93
SCN2	VT-A	1.63
SCN3	VT-B	0.93
SCN4	VT-B	1.63
SCN5	VT-C	0.93
SCN6	VT-C	1.63

Table 4. Identified ESI and absolute error of ELEM. No. 2 in sensitivity analysis

Damage Severity	Identified ESI	Theoretical ESI	Error(%)
D1	0.881	0.94	6.0
D2	0.774	0.80	2.6
D3	0.756	0.65	10.6

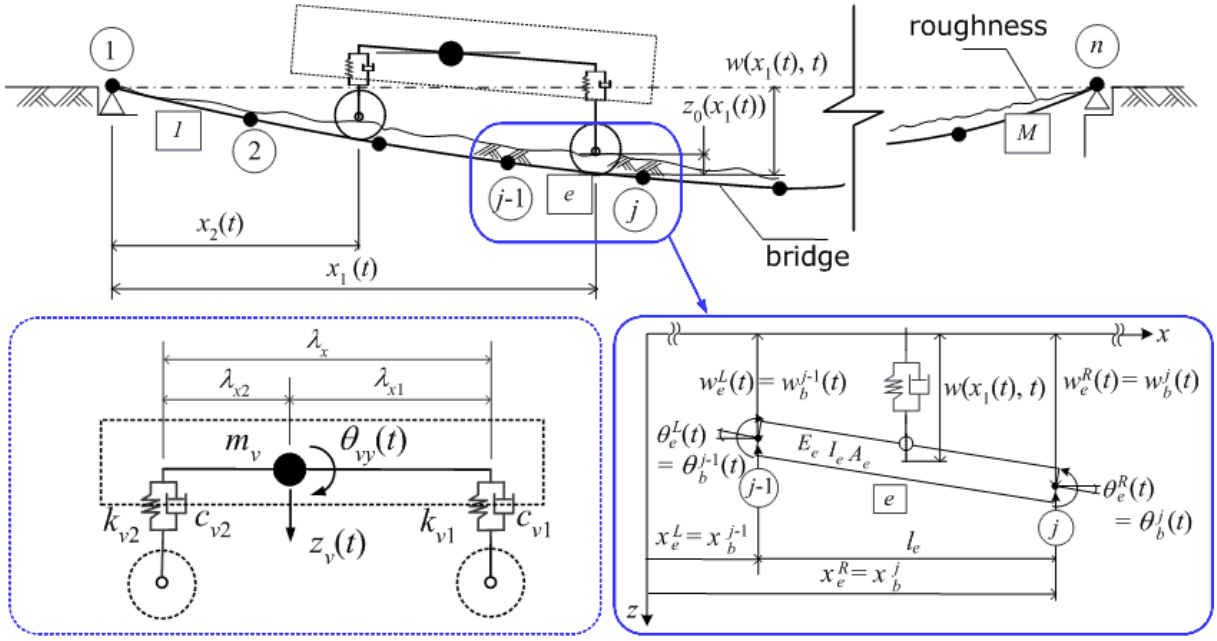

$z_v(t)$: Bounce motion,

$\theta_{vy}(t)$: Pitching motion

$w_e^R(t) = w_b^j(t)$: Vertical displacement at the right-hand side node of the e-th element (j-th node of the bridge)

$\theta_e^R(t) = \theta_b^j(t)$: Rotational angle at the right-hand side node of the e-th element (j-th node of the bridge)

$x_e^R = x_b^j$: Longitudinal coordinate of the right-hand side node of the e-th element (j-th node of the bridge)

E_e : Young's modulus of the e-th element

I_e : Inertia moment of the e-th element

A_e : Cross-sectional area of the e-th element

(j) : j-th node

$[e]$: e-th element

Figure 1. Scheme of a bridge-vehicle interactive system in moving vehicle laboratory experiment.

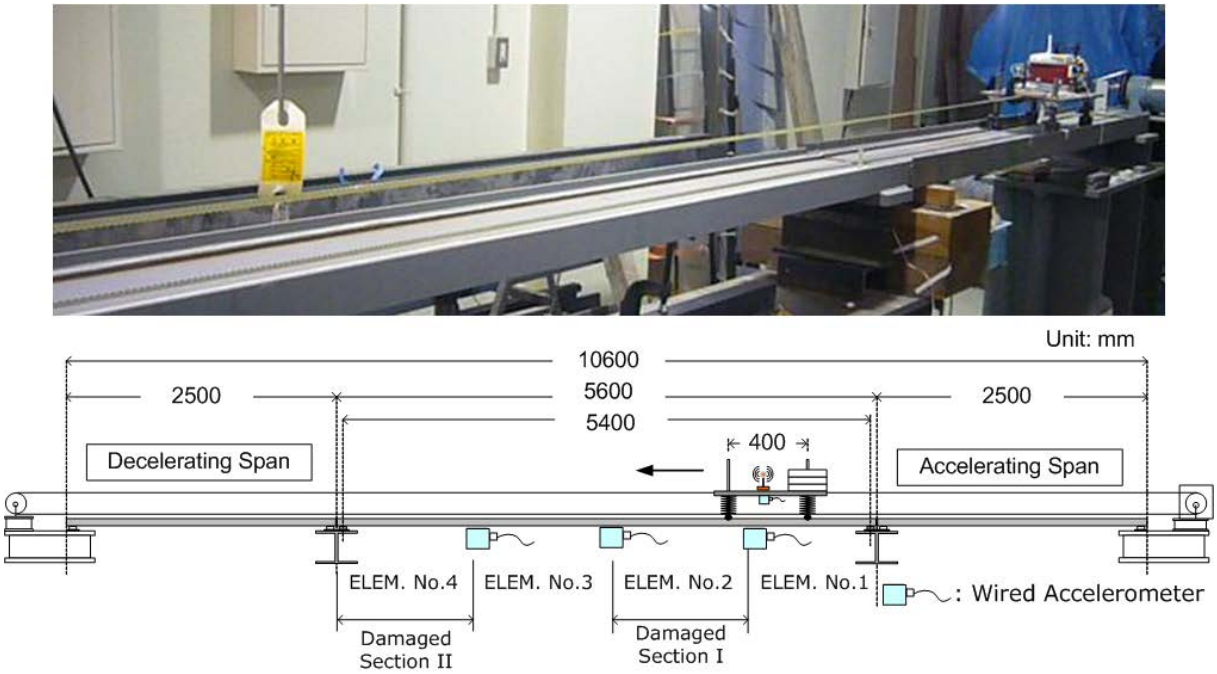

(a)

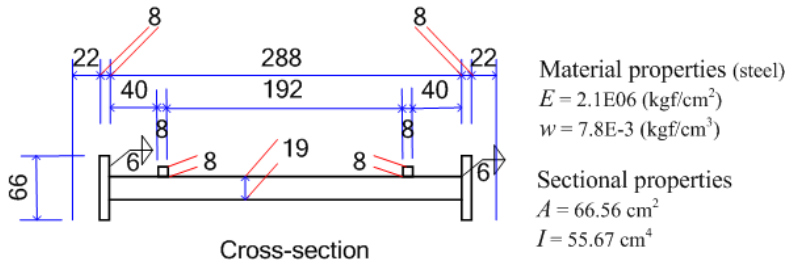

(b)

Figure 2. Experimental setup: (a) layout of experiment; (b) cross section of experiment girder; (c) damages; (d) damage scenarios.

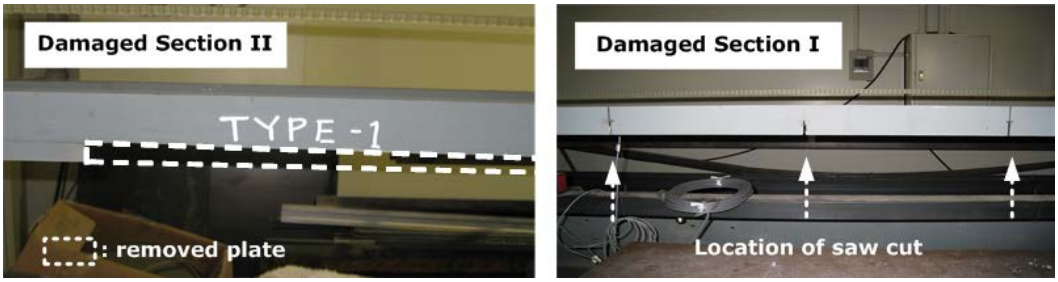

(c)

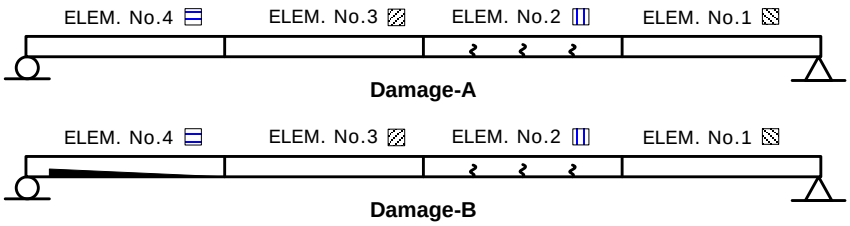

(d)

Figure 2. (Continued).

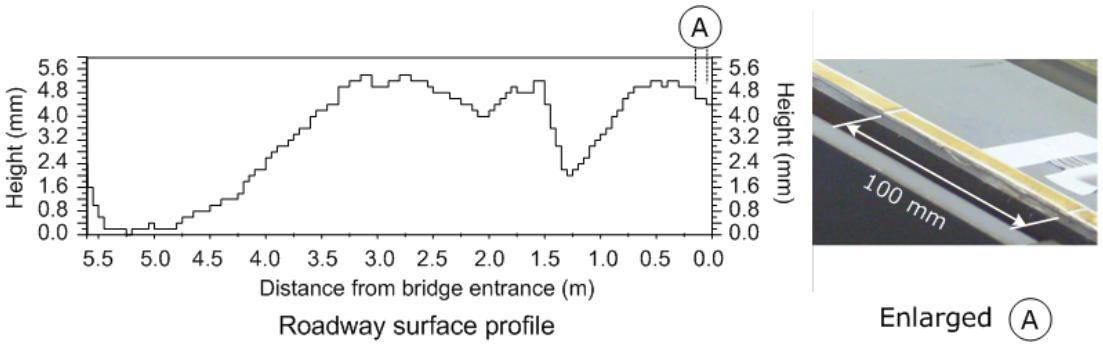

Figure 3. Roadway roughness on experimental girder.

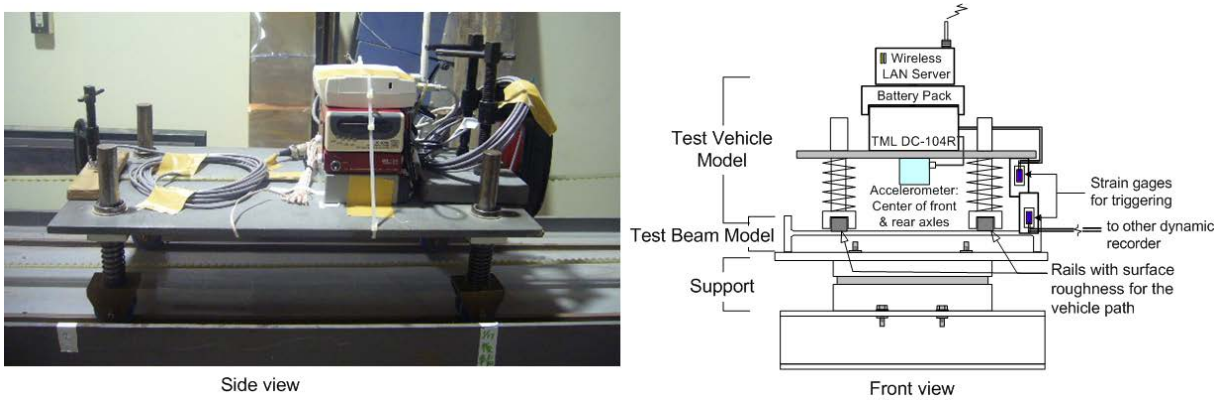

Figure 4. Experimental vehicle.

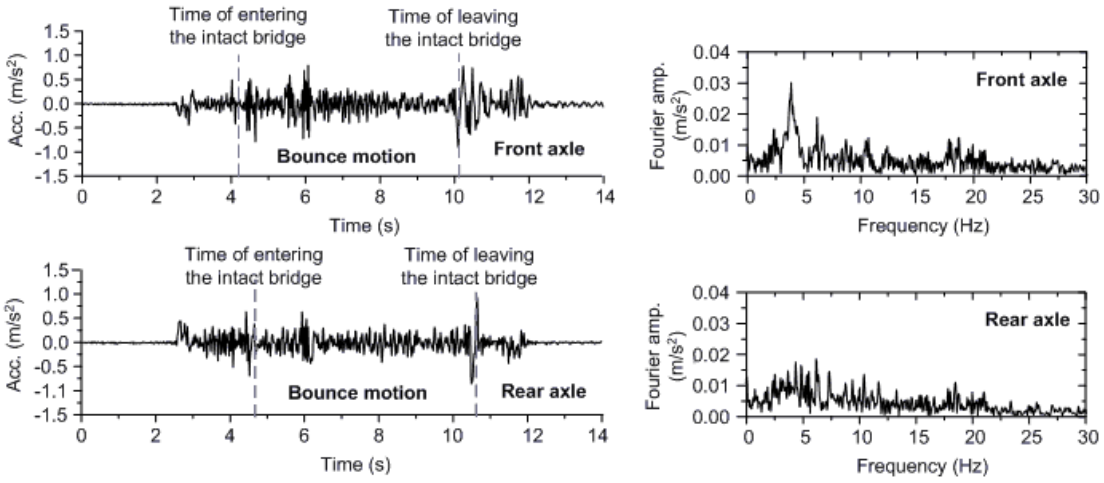

(a)

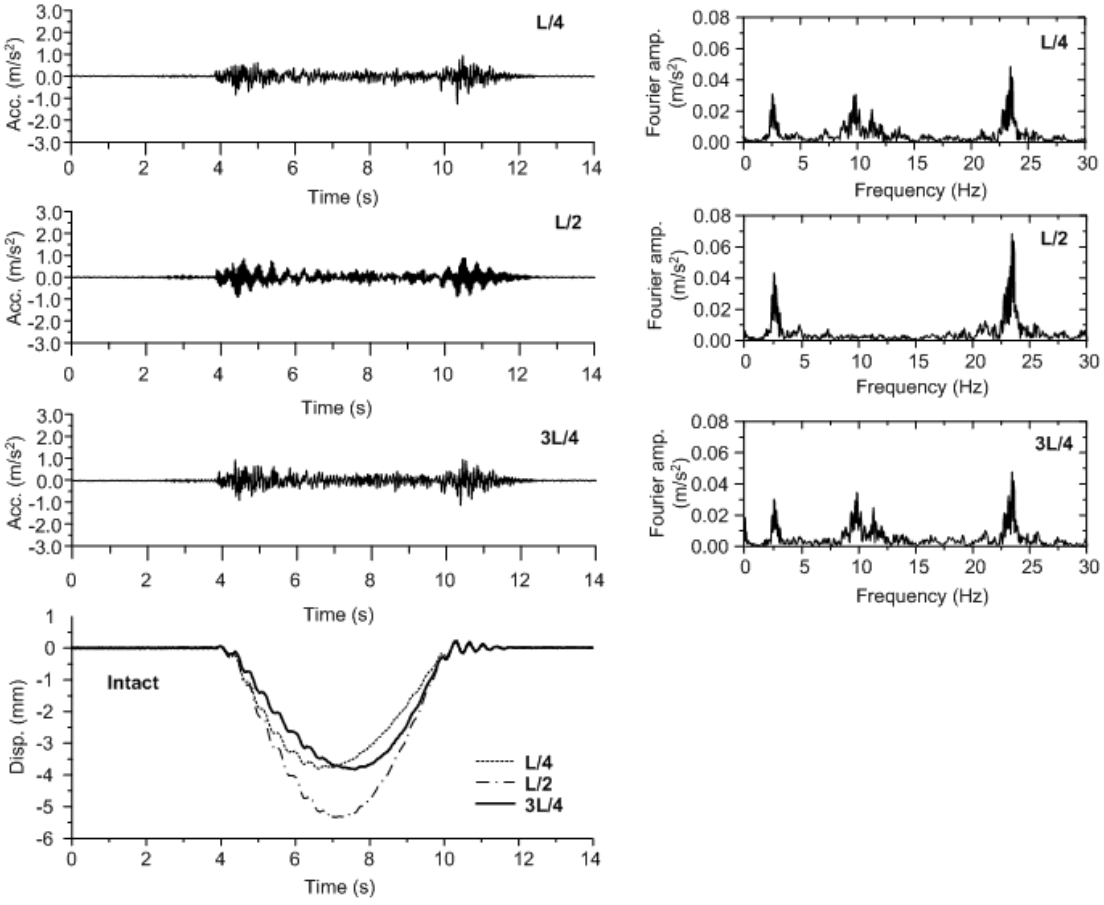

(b)

Figure 5. Dynamic responses of intact bridge and vehicle under loading scenario 1 (SCN1): (a) acceleration responses of vehicle; (b) acceleration and displacement responses of girder.

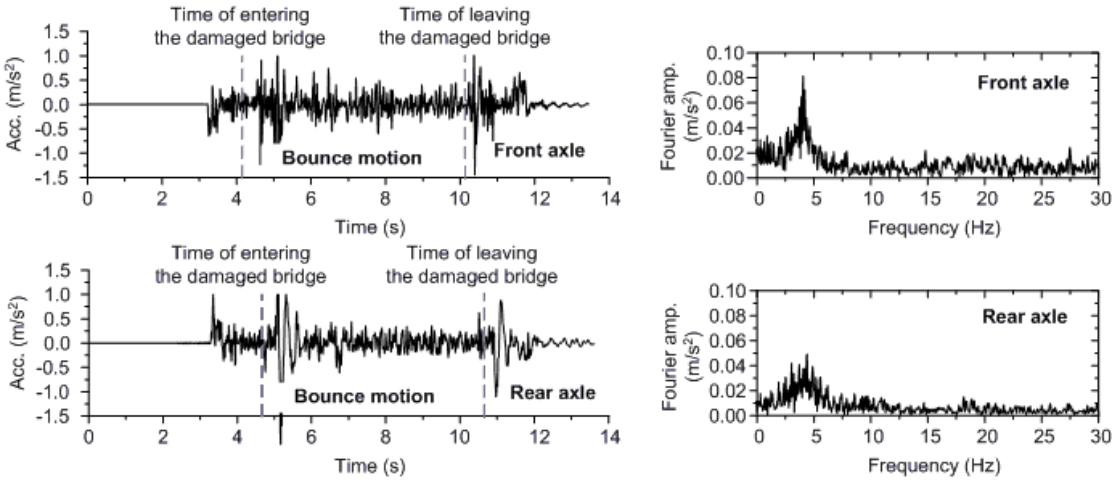

(a)

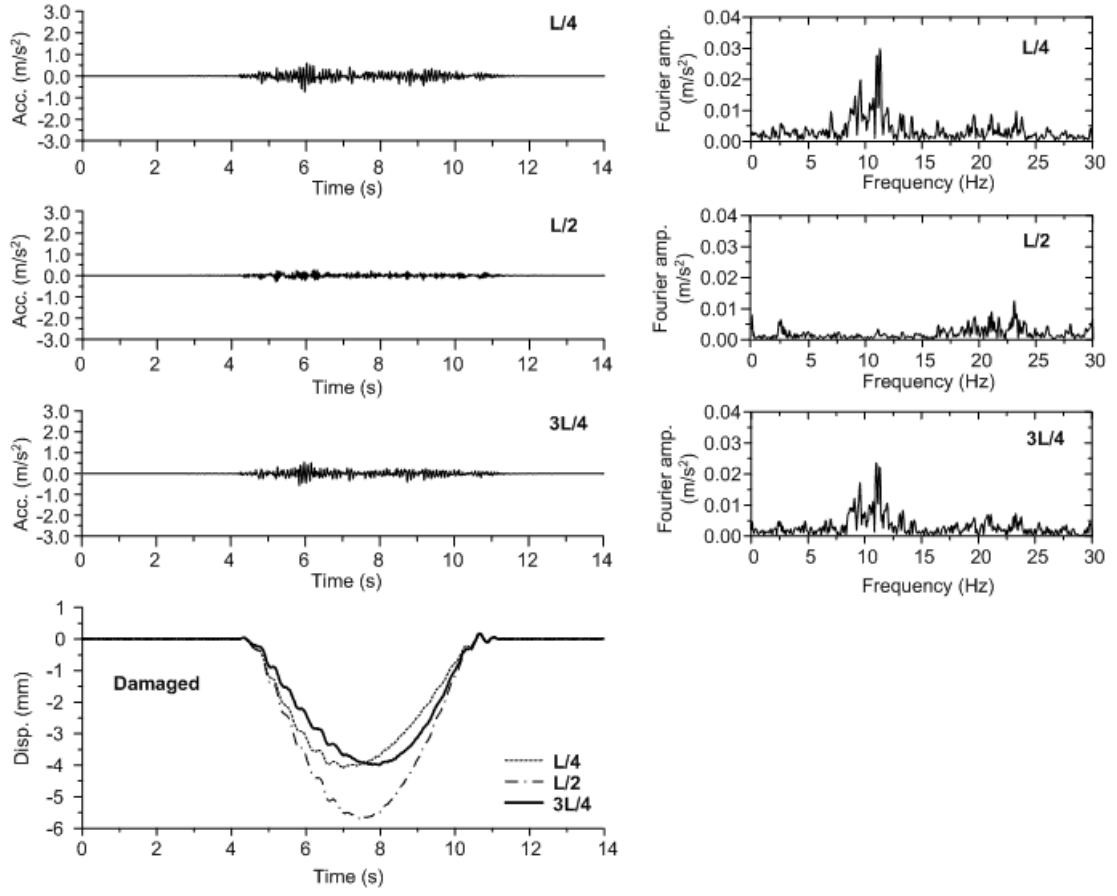

(b)

Figure 6. Dynamic responses of bridge and vehicle under damage scenario 1 and loading scenario 1 (SCN1): (a) acceleration responses of vehicle; (b) acceleration and displacement responses of girder.

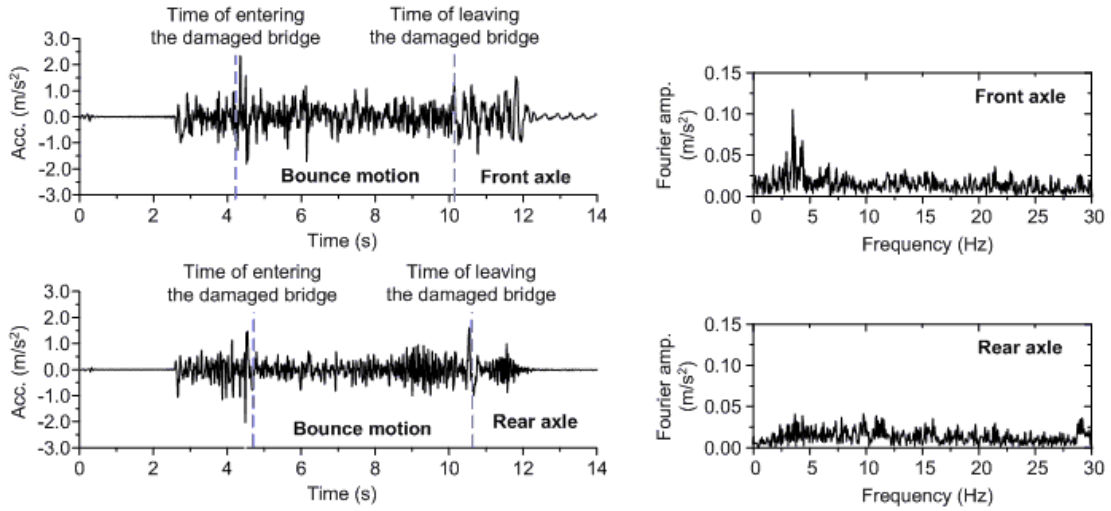

(a)

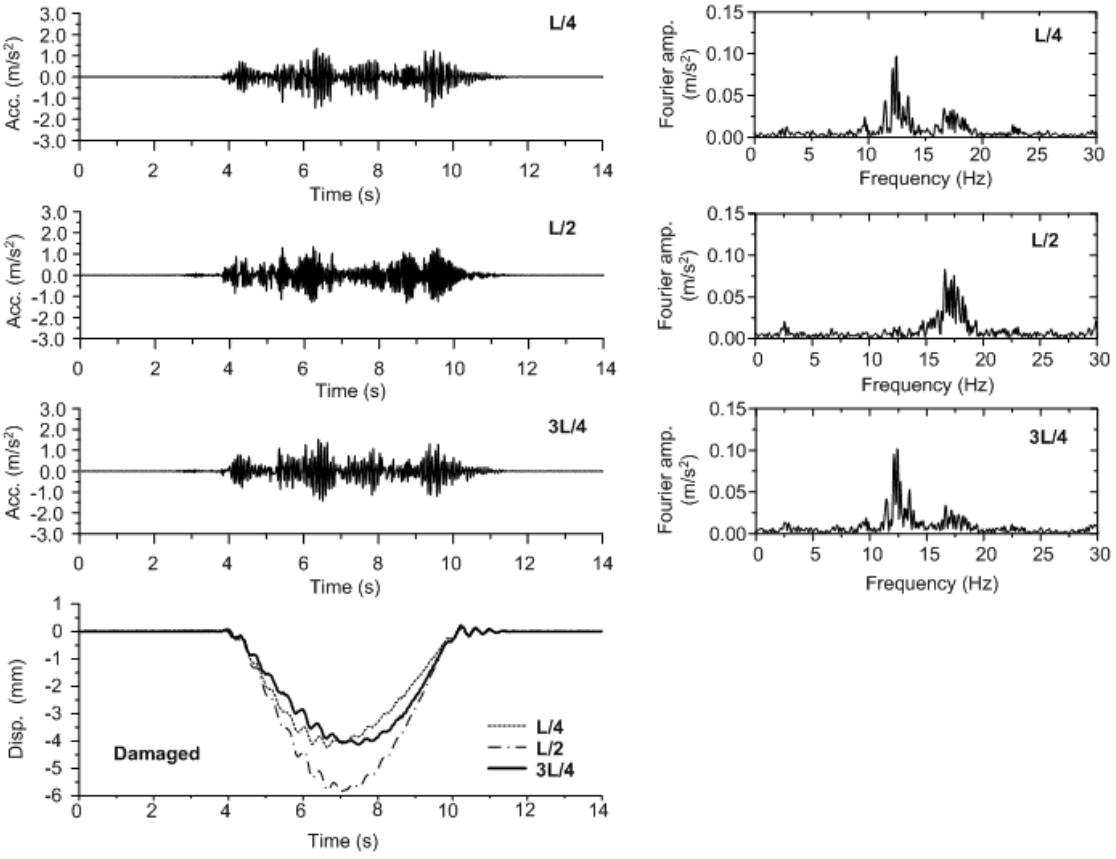

(b)

Figure 7. Dynamic responses of bridge and vehicle under damage scenario 2 and loading scenario 1 (SCN1): (a) acceleration responses of vehicle; (b) acceleration and displacement responses of girder.

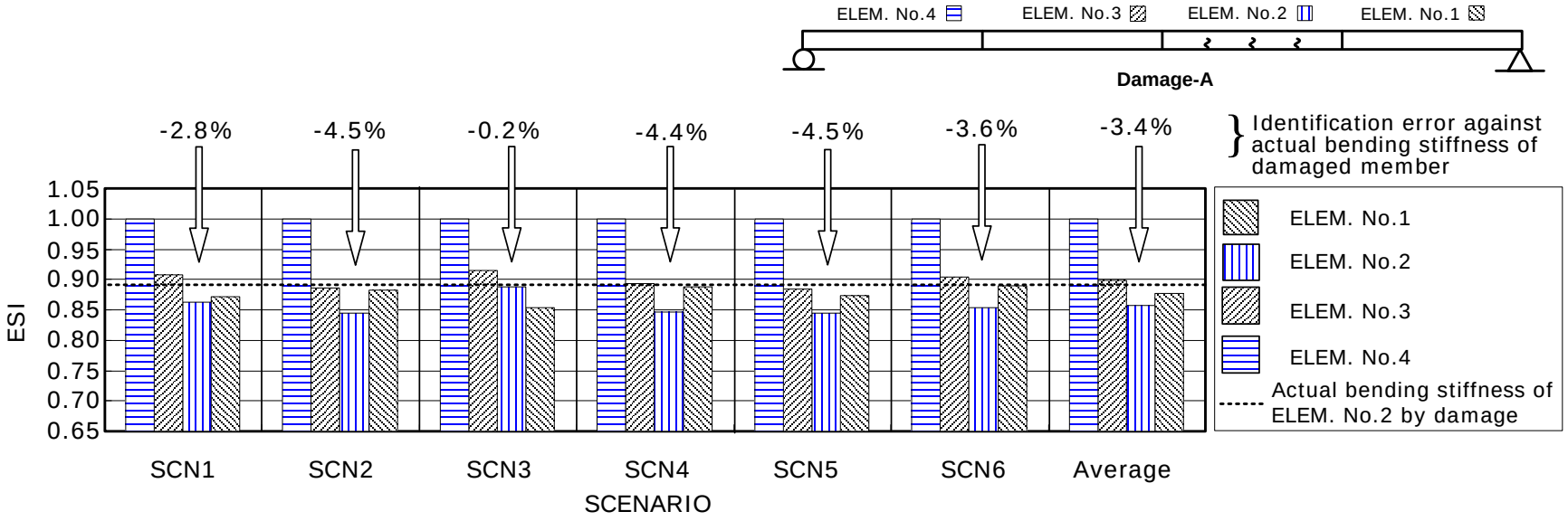

Figure 8. Identified damage location and severity of the bridge with damage at ELEM. No.2 (Damage-A) according to each traffic scenario.

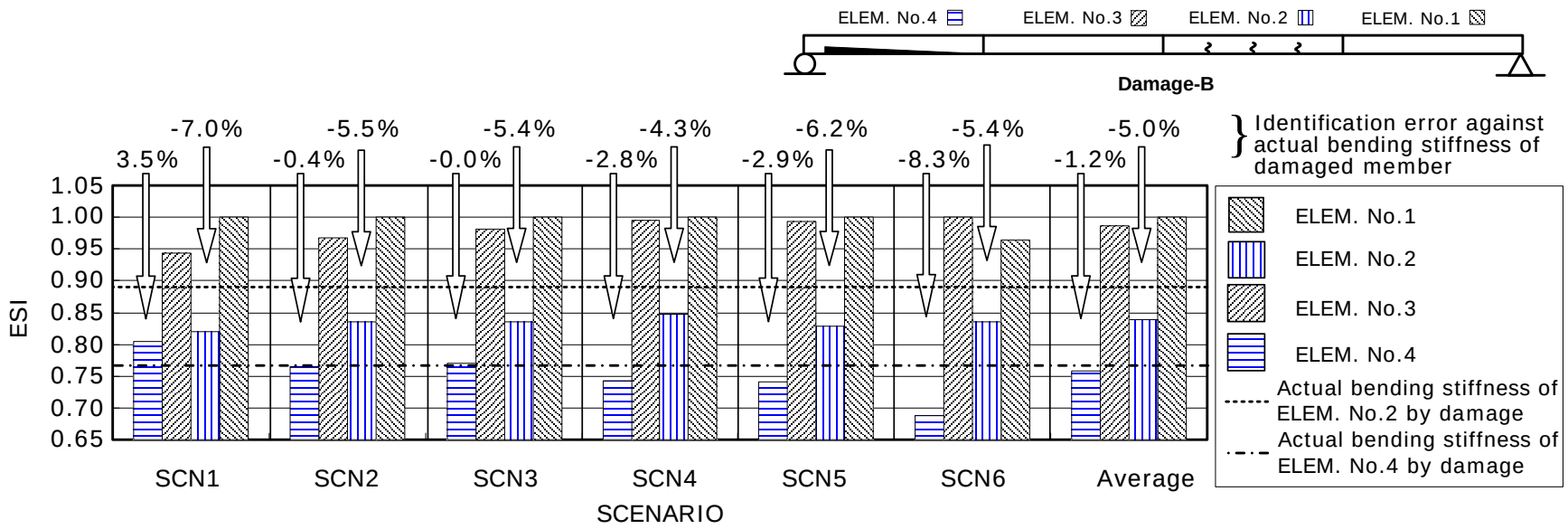

Figure 9. Identified damage location and severity of the bridge with damages at ELEM. No.2 and ELEM.4 (Damage-B) according to each traffic scenario.

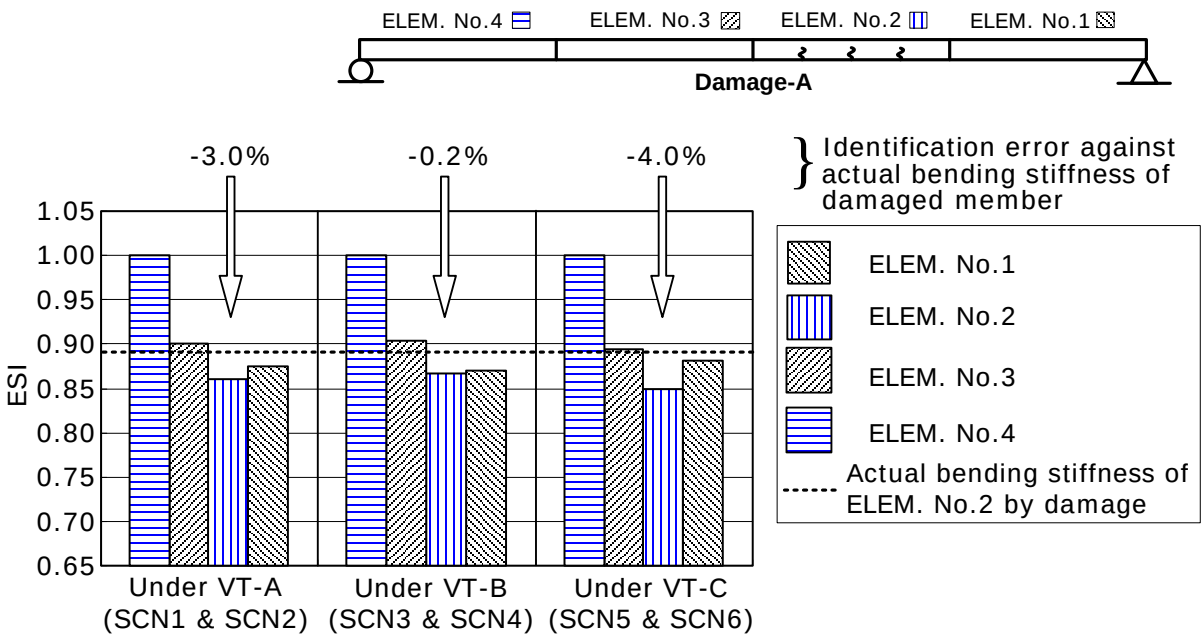

(a)

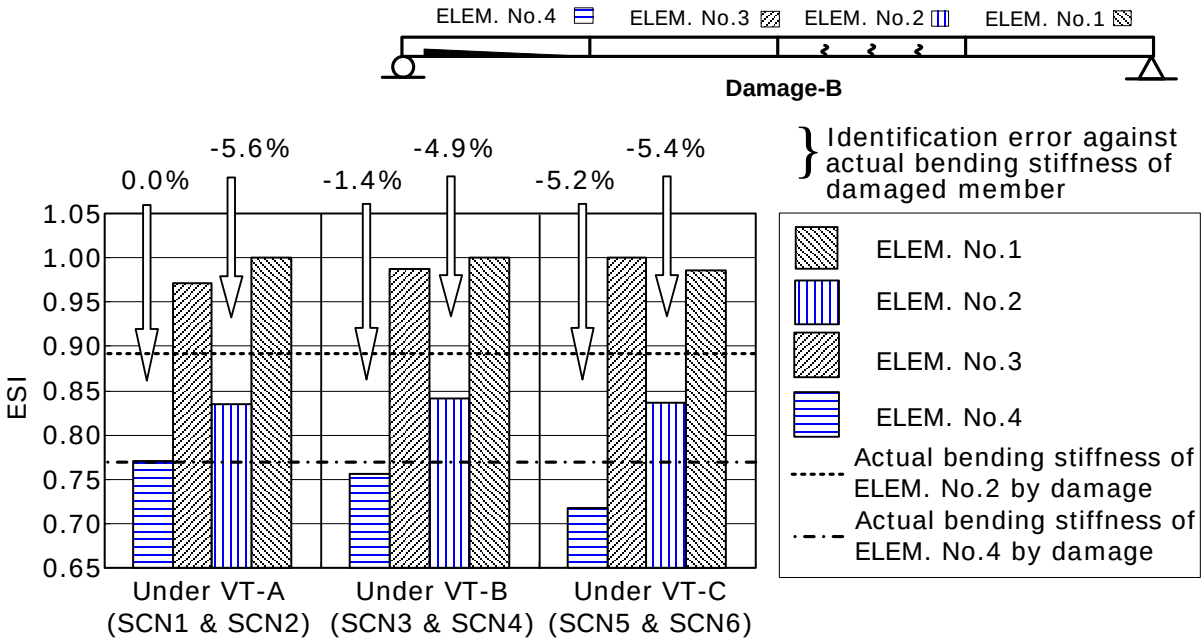

(b)

Figure 10. Identified damage location and severity of the bridge according to vehicle type: (a) with damage at ELEM. No.2 (Damage-A); (b) with damages both at ELEM. No.2 and ELEM. No.4 (Damage-B).

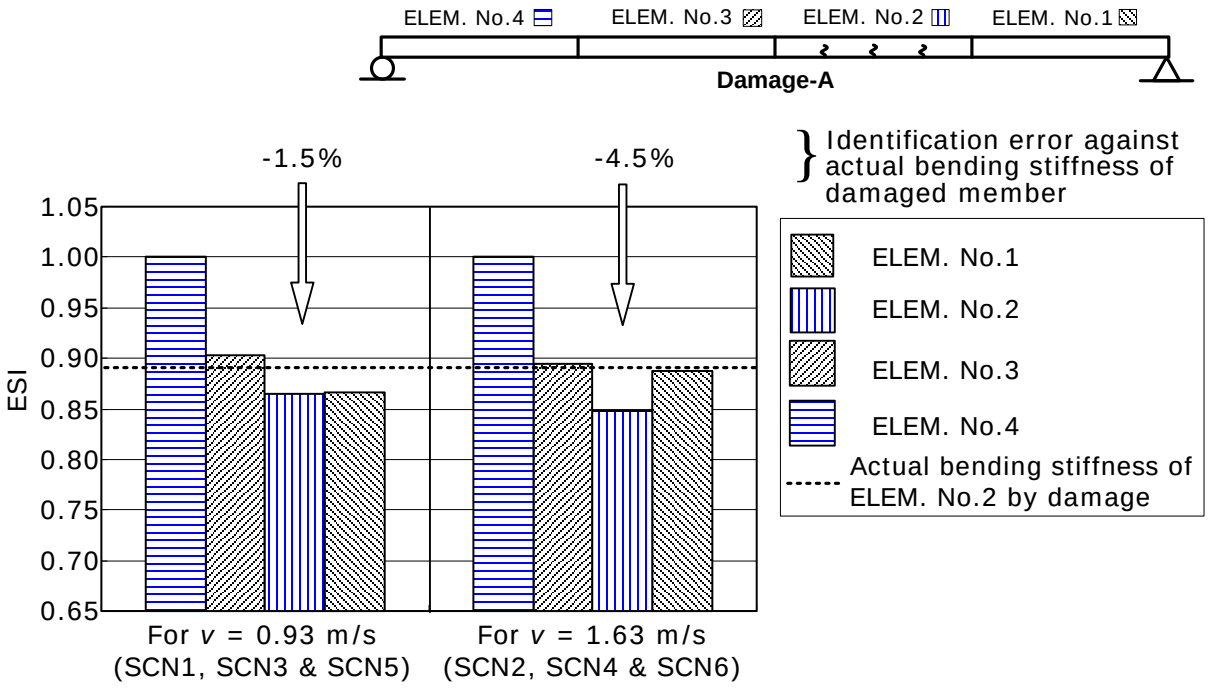

(a)

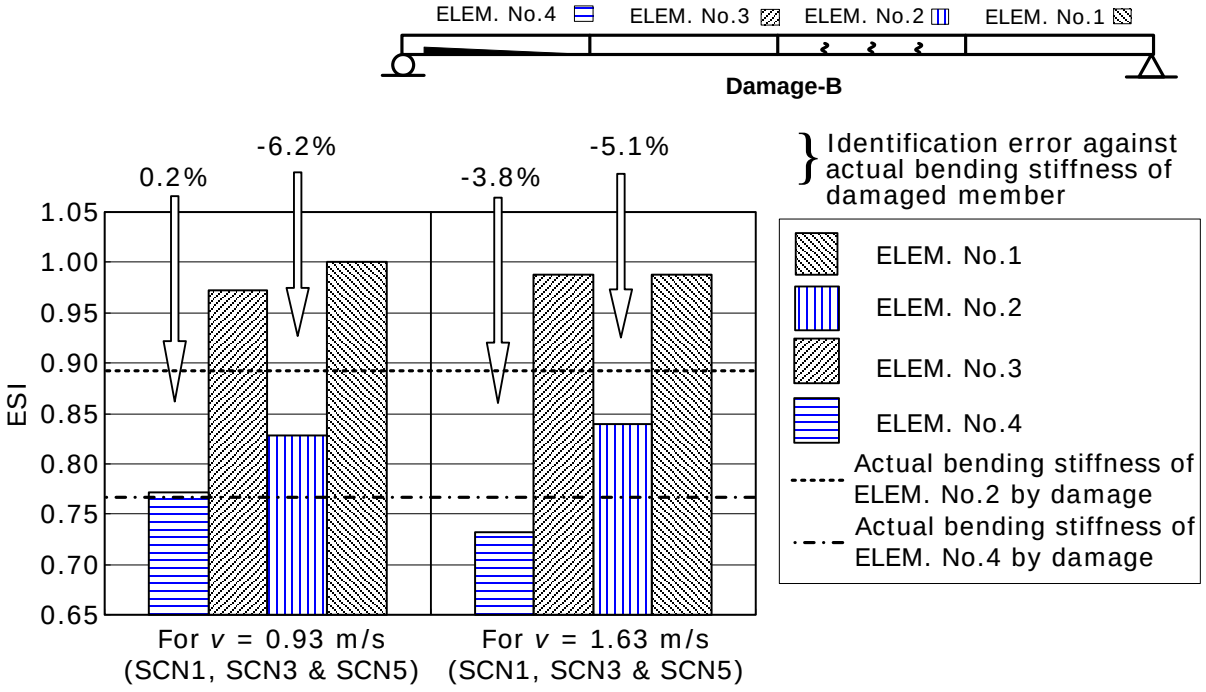

(b)

Figure 11. Identified damage location and severity of the bridge according to vehicle speed: (a) with damage at ELEM. No.2 (Damage-A); (b) with damages both at ELEM. No.2 and ELEM. No.4 (Damage-B).

Figure 12. Roadway roughness profile on the experiment girder in the sensitivity analysis.

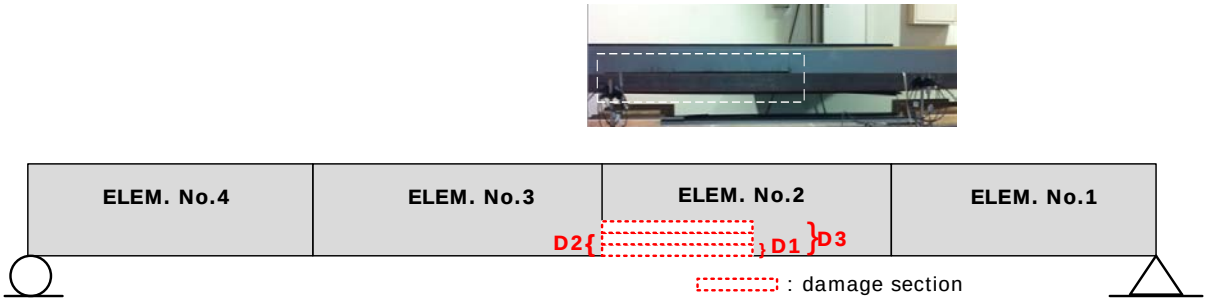

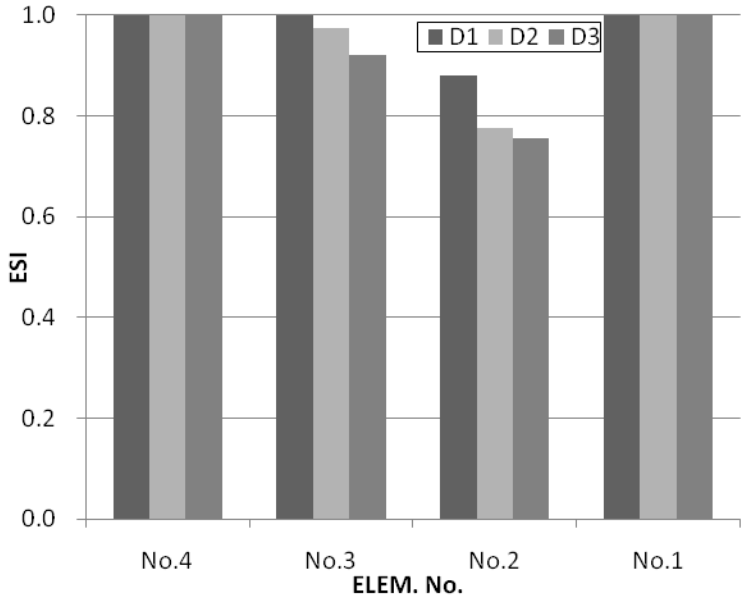

Figure 13. Identified ESI in the sensitivity analysis.